ACS OMEGA

http://pubs.acs.org/journal/acsodf

Article

Ni−Fe Cocatalysts on Magnesium Silicate Supports for the Depolymerization of Kraft Lignin

Apirat Laobuthee,* Anchan Khankhuean, Pasinee Panith, Chatchai Veranitisagul, and Navadol Laosiripojana*

Cite This: *ACS Omega* 2023, 8, 8675−8682

Read Online

ACCESS | Metrics & More | Article Recommendations

ABSTRACT: This research aimed to synthesize magnesium silicate ($MgSiO_3$) used as a support for Ni−Fe cocatalysts in the depolymerization of kraft lignin. Magnesium silicate was prepared by a hydrothermal method, followed by metal solution impregnation to obtain lignin depolymerization catalysts. The catalytic efficiency of kraft lignin depolymerization to valued phenolic compounds was studied by varying the ratios of Ni and Fe on the $MgSiO_3$ support. Moreover, other factors such as temperature, reaction time, and catalyst recycling affected both the quality and quantity of the products studied. The results illustrated that the catalyst 10Ni10Fe/MS produced all lignin depolymerization products with the highest yield (14.29 wt %) using reaction conditions of 300 °C and 1 h. In addition, the main products were found to be catechol (11.38 wt %), guaiacol (1.51 wt %), and phenol (0.79 wt %). More importantly, the 10Ni10Fe/MS catalyst showed good reusability even after two recycling processes, and the obtained phenol and guaiacol were found to be 0.63 and 1.01 wt %, respectively.

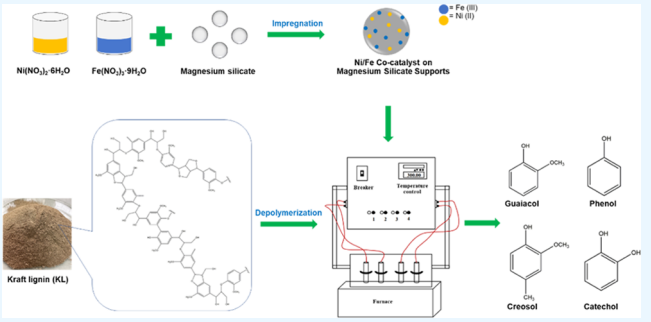

INTRODUCTION

Nowadays, the world is confronting concerns about global warming, rising populations, and the rapid depletion of fossil fuel reserves.[1,2] For these reasons, the requirements for sustainable industries based on renewable resources and low waste generation have increased. Consequently, the development of sustainable manufacturing fuels and chemicals from renewable resources must be addressed urgently.[3] Biomass is one of the most promising alternatives for energy and chemical raw materials due to its renewable, carbon-neutral, and high productivity characteristics.[4] Currently, the most abundant biopolymer on earth is the residue of lignocellulose biomass. Lignocellulosic biomass is composed of three kinds of components, namely, cellulose (30−50%), hemicellulose (20−35%), and lignin (15−30%).[5,6] Several technologies have been developed and employed commercially to convert cellulose and hemicellulose into chemicals, pulp, and paper. On the other hand, lignin is a renewable bioresource containing natural aromatic rings and is not widely used because of its highly complex structure and stable C−C bonds that result in difficulty when converting.[7] Lignin is classified into four types including kraft lignin (KL), soda lignin, lignosulfonates, and organosolv lignin based on the chemical pretreatment methods used.[8] Among these, kraft lignin (KL) is a low-value byproduct obtained from the paper and pulp industry, accounting for approximately 70 million metric tons.[9] Ultimately, KL is transferred to a boiler for burning with lower efficiency. This approach to the disposal of KL could lead to a mountain of solid waste in the future.[10]

Up to now, several methods for kraft lignin conversion have been widely explored, including biological methods, physical methods, and chemical methods.[11,12] Among these methods, the chemical method has gained interest from researchers and can be classified into pyrolysis, hydrogenolysis, liquid-phase reforming, gasification, and oxidation.[13−15] Even though the chemical approach efficiently transforms lignin into chemicals and liquid fuels, the three-dimensional amorphous structure of kraft lignin and the highly condensed and cross-linked C−C structures and β-ether units (like β-O-4) present the most challenging task that is difficult to overcome.[16,17] In addition, formation of the intermediate, which is strongly reactive during the depolymerization process, causes rapid repolymerization into heavy products.[12] To solve these problems, a diverse array of catalysts have been used for breaking the ether linkages of

Received: December 18, 2022
Accepted: February 13, 2023
Published: February 22, 2023

lignin, including homogeneous acid catalysts, homogeneous base catalysts, and heterogeneous metal catalysts.

Heterogeneous catalysts based on metals are used extensively in the catalytic cracking of lignin and lignin model compounds because of their advantages in terms of selectivity, reusability, and lack of emission pollutants. Generally, metal catalysts are mainly precious metals like ruthenium,[18] platinum,[19] palladium,[20] etc. Although precious metals can provide many attractive features, the cost and limited amounts of natural noble metals are drawbacks. For this reason, many researchers have focused on using non-noble metals as catalysts for lignin depolymerization. In recent years, Ni-based bimetallic catalysts, such as Ni−Fe,[14] Ni−Cu,[21] and Ni−Mo,[22] have been explored and reported to be suitable for the hydrogenolysis of lignin. Noble metal-based catalysts provide high activity for reactant conversion and low sensitivity to carbon formation. However, their application is often limited because of their high price and low availability.[23] Hence, many types of research have been conducted to enhance the stability of Ni-based catalysts by selecting the support, changing the method of catalyst synthesis, varying the nature of supports, and adding promoters to the catalyst.[24−26] There are several supports, such as γ-Al_2O_3, αAl_2O_3, MgO, SiO_2, $MgAl_2O_4$, etc., that are used in the reforming process.[27−29]

Magnesium silicate (MS), a compound of magnesium oxide (MgO) and silicon dioxide (SiO_2), can be prepared via a precipitation reaction between a soluble metal silicate (e.g., sodium ortho-silicate, sodium metasilicate, or potassium silicate) and a soluble magnesium salt (e.g., magnesium sulfate, nitrate, or chloride). In terms of appearance, magnesium silicate occurs as a fine, white, odorless, tasteless powder free from grittiness.[30,31] Magnesium silicate has gained appeal from many research groups and has been applied in various approaches such as dry-reforming, hydrodeoxygenation (HDO), and ethanol-to-butadiene processes.[32,33] Ghods et al.[34] synthesized $MgSiO_3$ with a high surface area (619 m^2/g) by the hydrothermal method and applied it as support in dry and steam reforming of methane. It was found that catalytic performance improved with increasing nickel content up to 10 wt %. The Ni/$MgSiO_3$ catalyst has also shown high stability in the dry-reforming process. Zhu et al.[35] investigated the effect of metal type, including Ni, Cu, Fe, Zn, and Co, metal loading, and reaction temperature on catalytic performance. The results showed that the 10 wt % Ni-MgO−SiO_2 catalyst provided the best catalytic performance, giving a yield of 81.5% to C_5−C_{15} ketones and alcohols at 240 °C. Fang et al.[36] prepared bimetallic Ni−Fe nanoparticles supported on carbon nanotubes (CNTs) and performed the catalytic hydrodeoxygenation (HDO) of a lignin-derived model compound, guaiacol. It was found that the performance of guaiacol HDO depends on the chemical state and size of the metallic nanoparticles as well as the Ni−Fe atomic ratio.

In the present study, magnesium silicate was synthesized as a support for Ni−Fe cocatalysts for kraft lignin depolymerization via a hydrothermal process, followed by metal solution impregnation to obtain the lignin depolymerization catalysts. The synthesized catalysts were characterized by Fourier transform infrared spectroscopy (FTIR), X-ray diffraction (XRD), X-ray fluorescence spectroscopy (XRF), scanning electron microscopy (SEM), and Brunauer−Emmett−Teller (BET) analysis. Moreover, the catalytic efficiency for kraft lignin depolymerization to valued phenolic compounds by varying the ratios of Ni and Fe on the $MgSiO_3$ support, along with other factors such as temperature, reaction time, and catalyst recycling that affected both the quality and quantity of products, was also studied.

MATERIALS AND METHODS

Materials. Magnesium nitrate hexahydrate ($Mg(NO_3)_2 \cdot 6H_2O$) was purchased from Merck. Sodium silicate (Na_2SiO_3) was purchased from TIAN-NAM Chemical Industrial Trade. Nickel nitrate hexahydrate ($Ni(NO_3)_2 \cdot 6H_2O$) was purchased from Carlo Erba and iron nitrate nonahydrate ($Fe(NO_3)_3 \cdot 9H_2O$) was purchased from Alpha Chemika. Propylene glycol-400 (commercial grade) was obtained from Suksapanpanit Thailand. The lignin source, an alkaline lignin powder with low sulfonate content, was obtained from Sigma-Aldrich and used without further purification.

Methods. *Preparation of Magnesium Silicate Supports ($MgSiO_3$).* Magnesium silicate (MS) was prepared via a hydrothermal method as follows: Na_2SiO_3, with a volume of 0.9 mL, was dissolved in water, while 1.48 g of $Mg(NO_3)_2 6H_2O$ was dissolved in a mixture of propylene glycol-400 and ethanol at a volume ratio of 3 to 1. After the two solutions were mixed, a white precipitate was observed. The pH of the mixture was further adjusted to 10 and stirred continuously for 30 min. The obtained mixture was transferred into an autoclave and treated at 150 °C for 24 h. Then, the obtained samples were filtered, washed with distilled water several times, dried at 80 °C overnight, and then further calcined at 800 °C for 6 h.

Preparation of Ni−Fe Cocatalysts on Magnesium Silicate Supports. In this study, Ni−Fe cocatalysts on magnesium silicate (MS) supports were synthesized via the microwave-assisted impregnation method. The Ni−Fe/MS was prepared by varying the ratios of Ni and Fe as 20Ni/MS, 15Ni5Fe/MS, 10Ni10Fe/MS, 5Ni15Fe/MS, and 20Fe/MS. Nickel nitrate hexahydrate and iron nitrate nonahydrate were dissolved in 20 mL of deionized (DI) water. Afterward, the aqueous solution was poured into the magnesium silicate and sonicated in a sonic bath for 30 min. To remove the moisture, the obtained samples were dried in a microwave at a frequency of 500 W for 5 min. Finally, the products were calcined at 800 °C for 4 h.

Characterization of Ni−Fe Cocatalysts on Magnesium Silicate Supports. FTIR spectra were obtained from a Fourier transform infrared spectrophotometer (Bruker, Alpha FTIR spectrometer). All FTIR transmission spectra were recorded in the range of 4000−400 cm^{-1} at a resolution of 2 cm^{-1} with 64 scans.

X-ray diffraction analysis was carried out by using a Philips X'Pert diffractometer with Cu radiation. The anode current and the voltage of an X-ray generator were 30 mA and 40 kV, respectively. The scanning rate was 0.02°/min in the 2θ diffraction angle range from 10 to 90°.

Scanning electron microscopy (SEM) images were obtained with a scanning electron microscope (SEM, FEI, QUANTA 450) using a tungsten filament operating at 10 kV to examine the morphology of Ni/Fe cocatalysts on magnesium silicate support samples.

The chemical compositions of the samples were characterized by an XRF spectrometer (Horiba XGT-2000W) with an X-ray tube operated at 50 kV and 1 mA.

Nitrogen adsorption−desorption measurements were performed using a Micromeritics 3Flex surface area and porosity analyzer. The samples were degassed at 200 °C for 24 h before

https://doi.org/10.1021/acsomega.2c08045
ACS Omega 2023, 8, 8675−8682

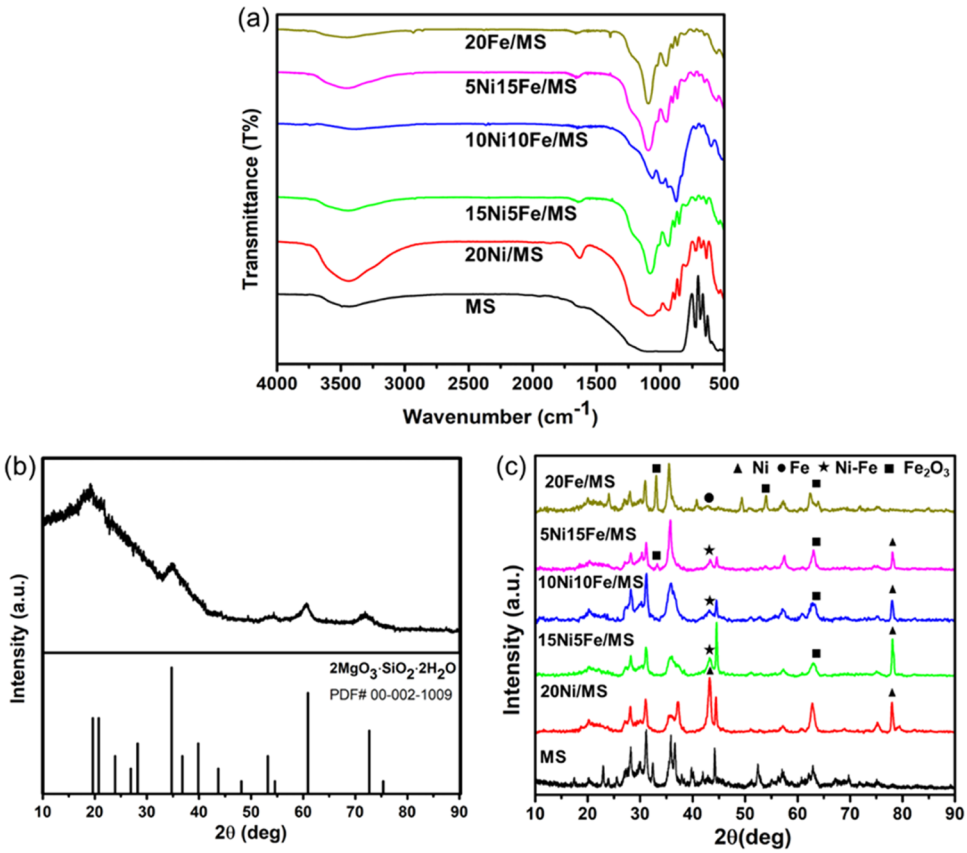

Figure 1. (a) FTIR spectra of magnesium silicate and Ni/Fe cocatalysts on magnesium silicate supports; (b) XRD patterns of magnesium silicate; and (c) XRD patterns of Ni/Fe cocatalysts on magnesium silicate supports.

the nitrogen gas adsorption measurement. The specific surface area (S_{BET}) of the prepared powder was calculated based on the Brunauer–Emmett–Teller (BET) principle referring to the nitrogen adsorption isotherm at 77 K.

Depolymerization of Kraft Lignin. First, 0.0875 g of lignin was suspended in DI water with the Ni–Fe cocatalysts on magnesium silicate supports in a batch reactor. To study the effect of temperature on the depolymerization of kraft lignin, the system was studied at temperatures of 250, 300, and 350 °C. Catalysts were further loaded at 0.0044 g into the reactor. Subsequently, the reactor was sealed and purged with N_2 to remove any reactive air and achieve an inert atmosphere until reaching 10 bars of N_2. The reactor was operated for 1 h with vertical shaking at 40 rpm.

After completing the reaction, the products were separated by a centrifuge consisting of solid and liquid phases. The solid phase was defined as char, while the liquid phase contained lignin-derived products and residual lignin. Next, the liquid phase was acidified to a pH of 2.00 with 1 M hydrochloric acid. In this step, the residual lignin was precipitated out as solids by a centrifuge at 15 °C. Next, the lignin-derived products were separated using ethyl acetate. Finally, the samples were characterized and quantified by a gas chromatography mass spectrometer.

The liquid fraction qualification was analyzed on a GC–MS instrument (Shimadzu) equipped with a capillary column (30 m × 0.32 mm × 0.25 mm). The GC heating ramp was as follows: the oven temperature program increased from 40 °C (held for 3 min) to 300 °C at a rate of 5 °C/min under a helium atmosphere. The main products from the depolymerization of kraft lignin are anisole, phenol, *p*-cresol, 4-ethylphenol, creosol, catechol, guaiacol, mequinol, 4-ethylguaiacol, syringol, 4-hydroxybenzaldehyde, vanillin, 4′-hydroxyacetophenone, 3,4-dimethoxyenzaldehyde, and vanillic acid. These products were analyzed using the database from the National Institute of Standards and Technology (NIST) for comparison of the molecular weight. The yields of each product and the kraft lignin conversion were calculated using the following eqs 1 and 2.

$$\text{yield} = \frac{\text{moles of product}}{\text{total moles of reactant}} \times 100\% \quad (1)$$

$$\text{conversion} = \frac{(\text{moles of reactant})_{in} - (\text{moles of reactant})_{out}}{(\text{moles of reactant})_{in}} \times 100\% \quad (2)$$

RESULTS AND DISCUSSION

Characterization of Ni–Fe Cocatalysts on Magnesium Silicate Supports. Figure 1a shows the FTIR spectra of magnesium silicate supports. The magnesium silicate supports show a broad peak at 3450 cm^{-1} attributed to the O–H stretching vibration of the moisture adsorbed on the surface of the magnesium silicate hydrate, while the absorption peak at 1641 cm^{-1}, corresponds to the Si–OH bending vibration. Moreover, the absorption peak at 1016 cm^{-1} is related to the symmetrical Si–O–Si stretching vibration. All vibration peaks of magnesium silicate agreed with the results presented by Iyad Rashid et al.[31] The FTIR spectra of Ni–Fe cocatalysts on

https://doi.org/10.1021/acsomega.2c08045
ACS Omega 2023, 8, 8675–8682

magnesium silicate supports with different ratios of Ni and Fe showed absorption peaks appearing at 426 and 724 cm^{-1}, indicating the functional groups of NiO[37] and Fe_2O_3,[38] respectively. The absorption peak at 1016 cm^{-1}, referred to as the symmetrical Si−O−Si stretching vibration, remains. It is notable that there is a slight shift in the bands/peaks of the O−H position due to the variation of the cation−oxygen bond length.[39,40] These results indicated that the impregnation of Ni−Fe metals on magnesium silicate supports did not affect the magnesium silicate structure.

The XRD patterns of magnesium silicate and Ni−Fe cocatalysts on magnesium silicate supports presented in Figure 1b correspond to the crystalline phase of magnesium silicate. These diffraction peaks were matched using the standard diffraction peaks of $MgSiO_3$ (JCPDS No. 00-002-0546). On the other hand, the main diffraction peaks of 20Fe/MS at 2θ 43.50° for Fe and 2θ 33.35, 55.90, and 62.30°, additionally observed, confirmed the formation of Fe_2O_3.[41] 20Ni/MS also showed diffraction peaks at 2θ 43.90, and 76.80°, indicating the existence of 111 and 220 planes of Ni, respectively.[42] In the case of 5Ni15Fe/MS, 10Ni10Fe/MS, and 15Ni5Fe/MS, the diffraction peak at 2θ 43.90° of Ni was slightly shifted to 43.70° when increasing the Fe content, indicating the formation of a Ni−Fe alloy for bimetallic 10Ni10Fe catalysts,[14,36] as depicted in Figure 1c. These XRD results indicated that Ni−Fe cocatalysts on magnesium silicate supports were successfully prepared by the hydrothermal process.

The Brunauer−Emmett−Teller (BET) equation was applied to calculate the specific area (S_{BET}), while the Barrer−Joyner−Halenda (BJH) equation was used to calculate the total pore volume and pore size distribution of the bimetallic catalysts. The magnesium silicate supports showed the highest surface area at 634.63 m^2/g, while the S_{BET} of the metallic catalysts at various ratios decreased significantly, as shown in Table 1.

Table 1. N_2 Adsorption−Desorption and t-Plot Analysis Results of the Materials

sample	S_{BET} (m^2/g)	total pore volume (cm^3/g)	average pore diameter (nm)
magnesium silicate	634.63	0.50	3.74
20Ni/MS	62.09	0.14	7.54
15Ni5Fe/MS	57.23	0.14	7.53
10Ni10Fe/MS	77.85	0.24	9.46
5Ni15Fe/MS	54.00	0.15	8.37
20Fe/MS	52.34	0.14	8.20

According to the SEM images in Figure 2, the microstructure of magnesium silicate exhibited a hierarchical structure and aggregation in some areas (Figure 2a). After loading metals via the impregnation method (Figure 2b), it was observed that the magnesium silicate pores were filled with metals, resulting in a decreased surface area.[43−45] All catalysts have a nearly similar surface area, pore volume, and pore size, which are 52−77 m^2/g, 0.14−0.24 cm^3/g, and 7.53−9.46 nm, respectively, due to the total metal loading of Ni−Fe being equal to 20% by mole. These results indicate that metal particles were successfully dispersed on the supports and entered the magnesium silicate pores. Moreover, a large pore diameter enables a better opportunity for feeding the molecules into the pores.

XRF analysis was carried out to determine the metal content of Ni and Fe contained in the Ni−Fe/MS catalysts. Table 2 confirms that the Ni−Fe bimetallic was successfully impregnated into the magnesium silicate supports. It was found that the percentage of metal contents was related to the prepared metal weight ratios. However, a slight error in metal content from the accurate content may be due to the XRF analysis, which analyzes the sample area in small points, resulting in the distribution of the metal weight ratio being slightly different.

Effect of Ni−Fe Ratios on Lignin Depolymerization. In this work, alkaline lignin was used to study the effect of Ni−Fe ratios on the magnesium silicate supports at 250 °C for 60 min. In Figure 3a, the total yield of the monometallic catalysts 20Ni/MS and 20Fe/MS was 1.64 and 3.73 wt %, respectively. The main products were guaiacol, vanillin, catechol, creosol, phenol, syringol, and 4-ethylguaiacol. In contrast, the bimetallic catalysts exhibited higher reactivity, and the total yields were also increased. The results revealed that the efficiency of bimetallic catalysts at 10Ni and 10Fe ratios provided the highest overall products. This may be due to the beneficial combination of Ni and Fe. Many types of research have reported on the advantages of Ni, such as thermal stability and catalytic activity. Moreover, Ni metal is an efficient hydrogenation metal for depolymerization reactions. Meanwhile, Fe has been used as an efficient catalyst in the reaction because Fe metal can weaken lignin's C−O binding ability. Another reason was that increasing the metal ratio resulted in increased productivity caused by the Fe metal acting as an acidic site.[46,47] Figure 3b shows the highest selectivity of guaiacol over other products. This could arise from the cleavage of the C−C bond in the 4-ethylguaiacol intermediate during guaiacol formation. It was found that the highest guaiacol was obtained with the 10Ni10Fe cocatalyst. Interestingly, syringol was derived when the Fe ratio was higher than 10 wt %. This may provide iron oxides in the Ni−Fe/MS catalyst, thus increasing acidic sites to promote the deoxygenation ability and enable better selectivity. These results also agree with those presented by Zhai et al.[14] So far, several researchers have reported the effect of the Ni−Fe ratio on various supports, such as activated carbon,[14] mesoporous carbon spheres,[41] and CeO_2−Al_2O_3.[48] The results revealed that Ni−Fe in a 1:1 ratio exhibited better performance in lignin depolymerization than the monometallic catalyst. Xiu et al.[48] proved that when the mass ratio of Ni−Fe is 1:1, the overall acidity is at its highest. This mass ratio can considerably promote the formation of alkaline lignin through a synergistic effect with metal Ni in the process of ether bond breaking.

Up to now, few researchers have investigated the metal or metal oxide on magnesium silicate supports. Yan et al.[49] studied the effect of catalysts on lignin depolymerization. It was found that the yield of monomer phenols (phenol-type, guaiacol-type, and syringol-type) of Ni−Fe−SiO_2 and Ni−Fe−Al_2O_3 was 16.19 and 19.01 wt %, respectively, which were close to our results. Due to its good catalyst performance, magnesium silicate can be used as a supported catalyst in lignin depolymerization.

Next we studied the part of the catalytic mechanism for lignin depolymerization by the Ni−Fe/MS catalyst. Dou et al.[50] reported the possibility of the role of Ni−Fe role in KL depolymerization using a hollow Ni−Fe catalyst. First, Fe attacks oxygen atoms and polarizes the C−O bonds in lignin; at the same time, Ni activates hydrogen. Then, the triggered hydrogen attacks the C−O−C and C−C bonds in KL, producing highly reactive deconstruction intermediates (e.g., coniferyl alcohols). These intermediates might either undergo

https://doi.org/10.1021/acsomega.2c08045
ACS Omega 2023, 8, 8675−8682

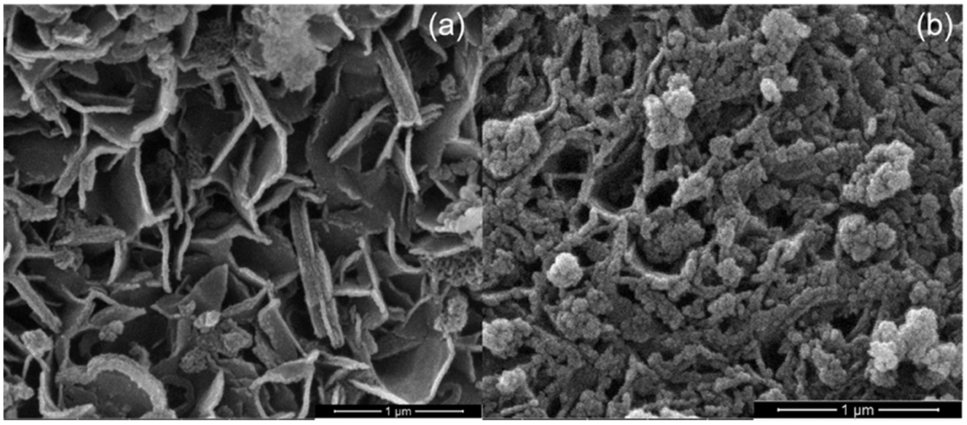

Figure 2. SEM images of (a) magnesium silicate and (b) Ni/Fe cocatalysts on magnesium silicate supports.

Table 2. XRF Analysis Data of the Ni/Fe Cocatalysts on Magnesium Silicate Supports

	elements (%)			
samples	Mg	Si	Ni	Fe
MS calcined	11.78	88.22		
20Ni/MS	15.46	54.45	29.84	0.12
15Ni5Fe/MS	14.66	62.00	18.02	5.32
10Ni10Fe/MS	34.08	48.03	9.64	8.25
5Ni15Fe/MS	0.26	67.99	14.10	17.65
20Fe/MS	46.56	45.18	0.01	8.26

condensation, which would result in the formation of repolymerized lignin fragments, or depolymerization, which would result in the construction of methoxyphenols. The presence of a hollow Ni−Fe catalyst also causes side-chain cleavage. For instance, the breakage of the C_α−C_{Ar} bond results in the production of guaiacol, while the removal of the hydroxyl groups from the C_α and C_γ positions generates propylguaiacol, eugenol, and isoeugenol, among other compounds.

Effect of Reaction Time on Lignin Depolymerization. Reaction time is another important factor affecting the yields of products from lignin. Here, 10Ni10Fe/MS was used to study the reaction time in the range of 30−150 min at 250 °C. From Figure 4, the results show that the overall product was found to be 5.68 wt % at 120 min of reaction time and the highest yield

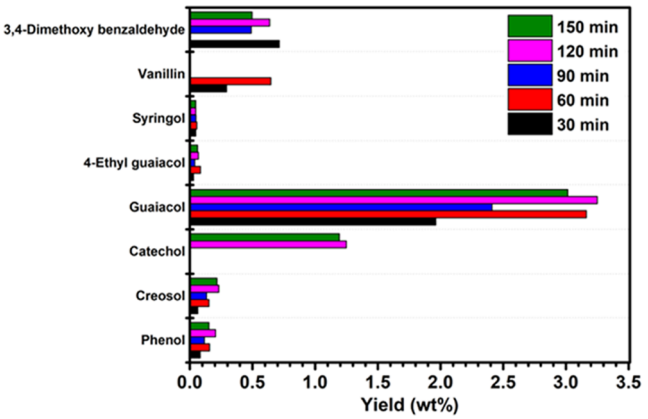

Figure 4. Yield of monomers at different reaction times.

product, guaiacol, was 3.25 wt %. In addition, the minor highest yield was found at 30 and 60 min for vanillin and at 120 and 150 min for catechol. However, the total yield at 90 min was lower than at 60 min, which may be due to the detection of intermediates during catechol formation. In

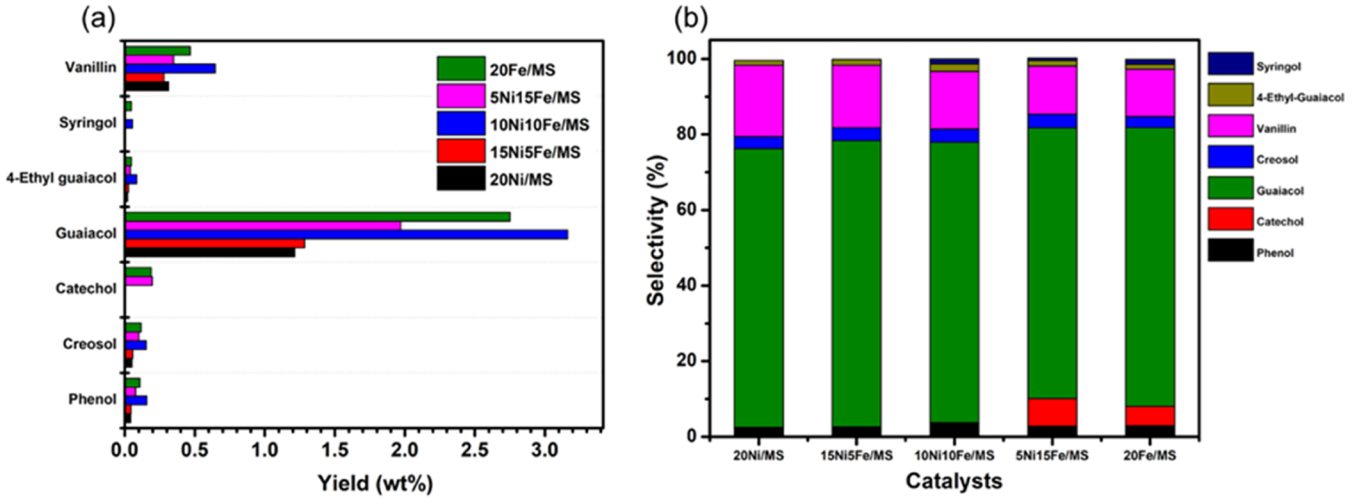

Figure 3. (a) Yields of monomers at different ratios of Ni−Fe metals on magnesium silicate and (b) selectivity of bimetallic catalysts at different ratios of Ni−Fe metals on magnesium silicate.

https://doi.org/10.1021/acsomega.2c08045
ACS Omega 2023, 8, 8675−8682

addition, increasing the reaction time in lignin depolymerization caused incremental yields of guaiacol, catechol, phenol, and 3,4-dimethoxy benzaldehyde. At 150 min of reaction time, the reduced total yield could arise from the char content being formed. This indicated that with a longer reaction time, more serious condensation reaction was found.

Investigation of Catalyst Stability. Considering the energy consumption, the catalyst recycling efficiency of materials was investigated further. The 10Ni10Fe/MS catalyst was tested at 250 °C for 60 min, after which the recycling time was studied, as shown in Figure 5. It was found that there was a 2-fold

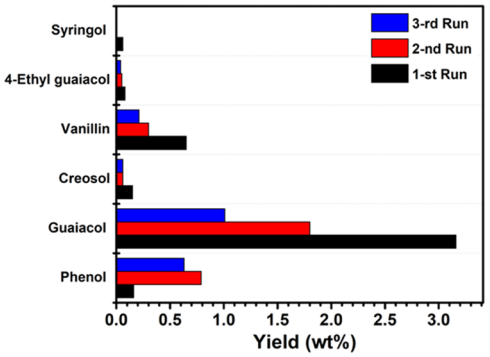

Figure 5. Yield of monomers at different recycling times.

reduction in guaiacol and vanillin yields after one recycling process. On the other hand, phenol contents were obtained by up to five times. After two recycles, the total yield was found to be lower than that obtained by using the catalyst in only one recycle. Moreover, the char content was higher compared to that from the first recycle. The results might be due to the aggregation of coke on the catalyst surface, resulting in a decrease in the total yield. Moreover, 10Ni10Fe/MS after recycling was analyzed by BET. The BET result shows that the surface area, total pore volume, and average pore diameter were 74.12 m^2/g, 0.22 cm^3/g, and 9.03 nm, respectively. These results revealed that the surface area and porosity of the catalyst after recycling were not significantly different from those of a fresh Ni−Fe catalyst. Therefore, the BET analysis can confirm that the catalyst deactivation of 10Ni10Fe/MS during recycling is low level.

Effect of Reaction Temperature on Lignin Depolymerization. It should be noted that temperature is one of the factors influencing the degree of lignin depolymerization. In this study, 10Ni10Fe/MS was used for analysis at 250, 300, and 350 °C for 60 min. From Figure 6, the highest yield found at 300 °C was 11.38 wt % as catechol was not found at a lower temperature. This may be attributed to demethylation through the O-CH_3 bond followed by H-addition at the O position (Figure 7). In addition, guaiacol, phenol, and vanillin were also found at 300 °C. It was found that increasing the temperature resulted in an increase in phenol yield. Moreover, the yield of guaiacol decreased, resulting from the increment of the other products. These results are related to those of Hu et al.,[46] who reported that the yield of phenols increased at a temperature higher than 220 °C due to the cleavage of C_1−Cα bonds of the phenylpropyl structure derived from the division of the aryl ether bonds of lignin.

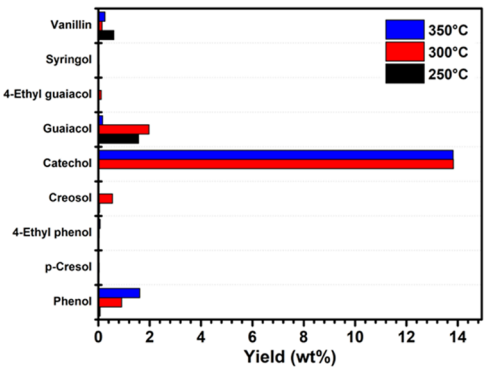

Figure 6. Yield of monomers at different reaction temperatures.

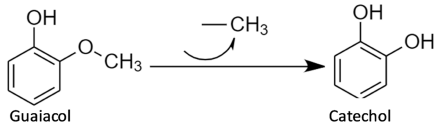

Figure 7. Demethylation of guaiacol.

CONCLUSIONS

Ni−Fe cocatalysts on magnesium silicate supports for the depolymerization of kraft lignin were prepared by the hydrothermal method, followed by metal solution impregnation. The obtained supports and lignin depolymerization catalysts were characterized by FTIR, XRD, BET, SEM, and XRF analyses. The decrease in the surface area of the bimetallic catalysts confirmed the success of the impregnation process in filling up $MgSiO_3$ support pores. It was found that the Ni and Fe ratio of 10:10 on magnesium silicate supports provided the highest total yield of valued phenolic compounds. In addition, reaction conditions, including temperature and time, influenced lignin depolymerization. It was found that the highest total yield of monomers from kraft lignin was 14.29 wt % at a temperature of 300 °C for 60 min. Moreover, the 10Ni10Fe/MS catalyst showed good reusability for two recycling processes, and the obtained phenol and guaiacol were 0.63 and 1.01 wt %, respectively. These results could be applied as a guideline for finding novel and efficient nonprecious metal catalysts in the future.

AUTHOR INFORMATION

Corresponding Authors

Apirat Laobuthee − *Department of Materials Engineering, Faculty of Engineering, Kasetsart University, Bangkok 10900, Thailand;* orcid.org/0000-0001-9744-9864; Email: fengapl@ku.ac.th

Navadol Laosiripojana − *The Joint Graduate School of Energy and Environment, King Mongkut's University of Technology Thonburi, Bangkok 10140, Thailand;* Email: navadol.lao@kmutt.ac.th

Authors

Anchan Khankhuean − *Department of Materials Engineering, Faculty of Engineering, Kasetsart University, Bangkok 10900, Thailand;* orcid.org/0000-0002-7980-3011

Pasinee Panith − *Department of Materials Engineering, Faculty of Engineering, Kasetsart University, Bangkok 10900, Thailand*

Chatchai Veranitisagul − *Department of Materials and Metallurgical Engineering, Faculty of Engineering,*

https://doi.org/10.1021/acsomega.2c08045
ACS Omega 2023, 8, 8675−8682

Rajamangala University of Technology Thanyaburi, Pathumthani 12110, Thailand; orcid.org/0000-0002-9280-1352

Complete contact information is available at: https://pubs.acs.org/10.1021/acsomega.2c08045

Notes

The authors declare no competing financial interest.

■ ACKNOWLEDGMENTS

This research was funded by the National Research Council of Thailand via the Kasetsart University Research and Development Institute (KURDI), FF (KU) 25.64. The authors would also like to thank Thailand's National Science and Technology Development Agency (NSTDA) for its facility support.

■ REFERENCES

(1) Rouches, E.; Gómez-Alvarez, H.; Majira, A.; Martín-Moldes, Z.; Nogales, J.; Díaz, E.; Bugg, T. D. H.; Baumberger, S. Assessment Strategy for Bacterial Lignin Depolymerization: Kraft lignin and Synthetic Lignin Bioconversion with Pseudomonas Putida. *Bioresour. Technol. Rep.* **2021**, *15*, No. 100742.

(2) Zhang, J.; Ge, Y.; Li, Z. Synchronous Catalytic Depolymerization of Alkaline Lignin to Monophenols with In situ-converted Hierarchical Zeolite for Bio-polyurethane Production. *Int. J. Biol. Macromol.* **2022**, *215*, 477−488.

(3) Wang, Y.; Tang, Z.; Chen, M.; Zhang, J.; Shi, J.; Wang, C.; Yang, Z.; Wang, J. Effect of Mo Content in Mo/Sepiolite Catalyst on Catalytic Depolymerization of Kraft Lignin Under Supercritical Ethanol. *Energy Convers. Manage.* **2020**, *222*, No. 113227.

(4) Erdocia, X.; Prado, R.; Fernández-Rodríguez, J.; Labidi, J. Depolymerization of Different Organosolv Lignins in Supercritical Methanol, Ethanol, and Acetone to Produce Phenolic Monomers. *ACS Sustainable Chem. Eng.* **2016**, *4*, 1373−1380.

(5) Kassaye, S.; Pant, K. K.; Jain, S. Hydrolysis of Cellulosic Bamboo Biomass into Reducing Sugars via a Combined Alkaline Solution and Ionic Liquid Pretreament Steps. *Renewable Energy* **2017**, *104*, 177−184.

(6) Mankar, A. R.; Ahmad, E.; Pant, K. K. Insights into Reductive Depolymerization of Kraft Lignin to Produce Aromatics in the Presence of Pt/HZSM-23 Catalyst. *Mater. Sci. Energy Technol.* **2021**, *4*, 341−348.

(7) Guan, W.; Chen, X.; Zhang, J.; Hu, H.; Liang, C. Catalytic Transfer Hydrogenolysis of Lignin α-O-4 Model Compound 4-(benzyloxy)phenol and Lignin over Pt/$HNbWO_6$/CNTs Catalyst. *Renewable Energy* **2020**, *156*, 249−259.

(8) Agarwal, A.; Jo, Y.-T.; Park, J.-H. Hybrid Microwave-ultrasound Assisted Catalyst-free Depolymerization of Kraft Lignin to Bio-oil. *Ind. Crops Prod.* **2021**, *162*, No. 113300.

(9) Huang, Y.; Duan, Y.; Qiu, S.; Wang, M.; Ju, C.; Cao, H.; Fang, Y.; Tan, T. Lignin-first Biorefinery: A Reusable Catalyst for Lignin Depolymerization and Application of Lignin Oil to Jet Fuel Aromatics and Polyurethane Feedstock. *Sustainable Energy Fuels* **2018**, *2*, 637−647.

(10) Jianfei, Y.; Zixing, F.; Liangmeng, N.; Qi, G.; Zhijia, L. Combustion Characteristics of Bamboo Lignin from Kraft Pulping: Influence of Washing Process. *Renewable Energy* **2020**, *162*, 525−534.

(11) Sun, Z.; Fridrich, B.; De Santi, A.; Elangovan, S.; Barta, K. Bright Side of Lignin Depolymerization: Toward New Platform Chemicals. *Chem. Rev.* **2018**, *118*, 614−678.

(12) Zhu, C.; Dou, X.; Li, W.; Liu, X.; Li, Q.; Ma, J.; Liu, Q.; Ma, L. Efficient Depolymerization of Kraft Lignin to Liquid Fuels over an Amorphous Titanium-zirconium Mixed Oxide Supported Partially Reduced Nickel-cobalt Catalyst. *Bioresour. Technol.* **2019**, *284*, 293−301.

(13) Sheng, X.; Li, S.; Zhao, Y.; Zhai, D.; Zhang, L.; Lu, X. Synergistic Effects of Two-dimensional MXene and Ammonium Polyphosphate on Enhancing the Fire Safety of Polyvinyl Alcohol Composite Aerogels. *Polymers* **2019**, *11*, 1964.

(14) Zhai, Y.; Li, C.; Xu, G.; Ma, Y.; Liu, X.; Zhang, Y. Depolymerization of Lignin via a Non-precious Ni−Fe Alloy Catalyst Supported on Activated Carbon. *Green Chem.* **2017**, *19*, 1895−1903.

(15) Li, C.; Zhao, X.; Wang, A.; Huber, G. W.; Zhang, T. Catalytic Transformation of Lignin for the Production of Chemicals and Fuels. *Chem. Rev.* **2015**, *115*, 11559−11624.

(16) Rinaldi, R.; Jastrzebski, R.; Clough, M. T.; Ralph, J.; Kennema, M.; Bruijnincx, P. C.; Weckhuysen, B. M. Paving the Way for Lignin Valorisation: Recent Advances in Bioengineering, Biorefining and Catalysis. *Angew. Chem., Int. Ed.* **2016**, *55*, 8164−215.

(17) Hao, G.; Liu, H.; Chang, Z.; Song, K.; Yang, X.; Ma, H.; Wang, W. Catalytic Depolymerization of the Dealkaline Lignin over Co−Mo−S Catalysts in Supercritical Ethanol. *Biomass Bioenergy* **2022**, *157*, No. 106330.

(18) (a) Shao, Y.; Xia, Q.; Dong, L.; Liu, X.; Han, X.; Parker, S. F.; Cheng, Y.; Daemen, L. L.; Ramirez-Cuesta, A. J.; Yang, S.; Wang, Y. Selective Production of Arenes via Direct Lignin Upgrading over a Niobium-based Catalyst. *Nat. Commun.* **2017**, *8*, No. 16104.

(19) Xia, Q.; Chen, Z.; Shao, Y.; Gong, X.; Wang, H.; Liu, X.; Parker, S. F.; Han, X.; Yang, S.; Wang, Y. Direct Hydrodeoxygenation of Raw Woody Biomass into Liquid Alkanes. *Nat. Commun.* **2016**, *7*, No. 11162.

(20) Onwudili, J. A.; Williams, P. T. Catalytic Depolymerization of Alkali Lignin in Subcritical Water: Influence of Formic acid and Pd/C Catalyst on the Yields of Liquid Monomeric Aromatic Products. *Green Chem.* **2014**, *16*, 4740−4748.

(21) Reddy Kannapu, H. P.; Mullen, C. A.; Elkasabi, Y.; Boateng, A. A. Catalytic Transfer Hydrogenation for Stabilization of Bio-oil Oxygenates: Reduction of P-cresol and Furfural over Bimetallic Ni−Cu Catalysts using Isopropanol. *Fuel Process. Technol.* **2015**, *137*, 220−228.

(22) Joshi, N.; Lawal, A. Hydrodeoxygenation of 4-Propylguaiacol (2-Methoxy-4-propylphenol) in a Microreactor: Performance and Kinetic Studies. *Ind. Eng. Chem. Res.* **2013**, *52*, 4049−4058.

(23) Zhu, J.; Peng, X.; Yao, L.; Tong, D.; Hu, C. CO_2 reforming of Methane over Mg-promoted Ni/SiO_2 catalysts: the Influence of Mg Precursors and Impregnation Sequences. *Catal. Sci. Technol.* **2012**, *2*, 529−537.

(24) Xu, L.; Song, H.; Chou, L. Carbon dioxide Reforming of Methane over Ordered Mesoporous NiO−MgO−Al_2O_3 Composite Oxides. *Appl. Catal., B* **2011**, *108*−*109*, 177−190.

(25) Al-Fatesh, A. S. A.; Fakeeha, A. H.; Abasaeed, A. E. Effects of Selected Promoters on Ni/Y-Al_2O_3 Catalyst Performance in Methane Dry Reforming. *Chin. J. Catal.* **2011**, *32*, 1604−1609.

(26) Arandiyan, H.; Li, J.; Ma, L.; Hashemnejad, S. M.; Mirzaei, M. Z.; Chen, J.; Chang, H.; Liu, C.; Wang, C.; Chen, L. Methane Reforming to Syngas over $LaNi_xFe_{1-x}O_3$ ($0\leq x\leq 1$) Mixed-oxide Perovskites in the Presence of CO_2 and O_2. *J. Ind. Eng. Chem.* **2012**, *18*, 2103−2114.

(27) Hu, Y. H. Solid-solution catalysts for CO_2 Reforming of Methane. *Catal. Today* **2009**, *148*, 206−211.

(28) Pérez-Moreno, L.; Soler, J.; Herguido, J.; Menéndez, M. Stable Hydrogen Production by Methane Steam Reforming in a Two-zone Fluidized-bed Reactor: Effect of the Operating Variables. *Int. J. Hydrogen Energy* **2013**, *38*, 7830−7838.

(29) Lisboa, J. d. S.; Santos, D. C. R. M.; Passos, F. B.; Noronha, F. B. Influence of the Addition of Promoters to Steam Reforming Catalysts. *Catal. Today* **2005**, *101*, 15−21.

(30) Krysztafkiewicz, A.; Lipska, L. K.; Ciesielczyk, F.; Jesionowski, T. Amorphous Magnesium Silicate-synthesis, Physicochemical Properties and Surface Morphology. *Adv. Powder Technol.* **2004**, *15*, 549−565.

(31) Rashid, I.; Daraghmeh, N.; Al Omari, M.; Chowdhry, B.; Leharne, S.; Hodali, H.; Badwan, A. Magnesium Silicate. In *Profiles of Drug Substances, Excipients and Related Methodology*; Academic Press, 2011; Vol. *36*, pp 241−285.

(32) Chung, S.-H.; Angelici, C.; Hinterding, S. O. M.; Weingarth, M.; Baldus, M.; Houben, K.; Weckhuysen, B. M.; Bruijnincx, P. C. A. Role of Magnesium Silicates in Wet-Kneaded Silica−Magnesia Catalysts for the Lebedev Ethanol-to-Butadiene Process. *ACS Catal.* **2016**, *6*, 4034−4045.
(33) Ochoa, J. V.; Malmusi, A.; Recchi, C.; Cavani, F. Understanding the Role of Gallium as a Promoter of Magnesium Silicate Catalysts for the Conversion of Ethanol into Butadiene. *ChemCatChem* **2017**, *9*, 1−7.
(34) Ghods, B.; Rezaei, M.; Meshkani, F. Ni Catalysts Supported on Mesoporous Nanocrystalline Magnesium Silicate in Dry and Steam Reforming Reactions. *Chem. Eng. Technol.* **2017**, *40*, 760−768.
(35) Zhu, Q.; Shen, C.; Wang, J.; Tan, T. Upgrade of Solvent-Free Acetone-Butanol-Ethanol Mixture to High-Value Biofuels over Ni-Containing MgO−SiO_2 Catalysts with Greatly Improved Water-Resistance. *ACS Sustainable Chem. Eng.* **2017**, *5*, 8181−8191.
(36) Fang, H.; Zheng, J.; Luo, X.; Du, J.; Roldan, A.; Leoni, S.; Yuan, Y. Product Tunable Behavior of Carbon Nanotubes-supported Ni−Fe Catalysts for Guaiacol Hydrodeoxygenation. *Appl. Catal., A* **2017**, *529*, 20−31.
(37) Rahdar, A.; Aliahmad, M.; Azizi, Y. NiO Nanoparticles: Synthesis and Characterization. *J. Nanostruct.* **2015**, *5*, 145−151.
(38) Abdulah, H. I.; Farhan, A.; Ali, A. Photo-synthesis of Nanosized α−Fe_2O_3. *J. Chem. Pharm. Res.* **2015**, *7*, 588−591.
(39) Mohammed, K. A.; Al-Rawas, A. D.; Gismelseed, A. M.; Sellai, A.; Widatallah, H. M.; Yousif, A.; Elzain, M. E.; Shongwe, M. Infrared and Structural Studies of $Mg_{1-x}Zn_xFe_2O_4$ ferrites. *Phys. B* **2012**, *407*, 795−804.
(40) Suman, S.; Chahal, S.; Kumar, A.; Kumar, P. Zn Doped α-Fe_2O_3: An Efficient Material for UV Driven Photocatalysis and Electrical Conductivity. *Crystals* **2020**, *10*, 273.
(41) Yazirin, C.; Puspitasari, P.; Sasongko, M. I. N.; Tsamroh, D. I.; Risdanareni, P. Phase Identification and Morphology Study of Hematite (Fe_2O_3) with Sintering Time Varitions. *AIP Conf. Proc.* **2017**, *1887*, No. 020038.
(42) Han, Q.; Rehman, M. U.; Wang, J.; Rykov, A.; Gutierrez, O. Y.; Zhao, Y.; Wang, S.; Ma, X.; Lerche, J. A. The Synergistic Effect between Ni Sites and Ni-Fe Alloy Sites on Hydrodeoxygenation of Lignin-derived Phenols. *Appl. Catal., B* **2019**, *253*, 348−358.
(43) Susmanto, P.; Gusman, Y.; Ridwan, M. F.; Tanara, E. H. Characterization of Cr/SiO_2/Al_2O_3 Catalyst from Rice Husk using Impregnation Method. *Indones. J. Chem. Anal.* **2020**, *3*, 33−39.
(44) Tomin, O.; Vahala, R.; Yazdani, M. R. Tailoring Metal-impregnated Biochars for Selective Removal of Natural Organic Matter and Dissolved Phosphorus from the Aqueous Phase. *Microporous Mesoporous Mater.* **2021**, *328*, No. 111499.
(45) Muna, I. A.; Kurniawansyah, F.; Mahfud, M.; Roesyadi, A. Synthesis and Characterization of Cr-Co/γ-alumina Catalyst for Ethanol Dehydration. *AIP Conf. Proc.* **2021**, *2349*, No. 020041.
(46) Hu, L.; Luo, Y.; Cai, B.; Li, J.; Tong, D.; Hu, C. The degradation of the lignin in Phyllostachys heterocycla cv. pubescens in an ethanol solvothermal system. *Green Chem.* **2014**, *16*, 3107−3116.
(47) Zhang, W.; Shi, X.; Gao, M.; Liu, J.; Lv, Z.; Wang, Y.; Huo, Y.; Cui, C.; Yu, Y.; He, H. Iron-Based Composite Oxide Catalysts Tuned by CTAB Exhibit Superior NH_3-SCR Performance. *Catalysts* **2021**, *11*, 1−14.
(48) Xiu, P.; Lu, X.; Wang, D.; Chen, J.; Xu, C.; Gu, X. Efficient Depolymerization of Alkaline Lignin to Phenolic Monomers over Non-precious Bimetallic Ni−Fe/CeO_2-Al_2O_3 Catalysts. *Biomass Convers. Biorefin.* **2022**, 1−16.
(49) Yan, B.; Lin, X.; Chen, Z.; Cai, Q.; Zhang, S. Selective Production of Phenolic Monomers via High Efficient Lignin Depolymerization with a Carbon Based Nickel-Iron-Molybdenum carbide Catalyst under Mild Conditions. *Bioresour. Technol. Rep.* **2021**, *321*, No. 124503.
(50) Dou, X.; Li, W.; Zhu, C.; Jiang, X. Catalytic Waste Kraft Lignin Hydrodeoxygenation to Liquid Fuels over a Hollow Ni-Fe Catalyst. *Appl. Catal., B* **2021**, *287*, 119−975.

https://doi.org/10.1021/acsomega.2c08045
ACS Omega 2023, 8, 8675−8682